An advanced oxy-fuel power cycle with high efficiency

C Gou[1,2]*, **R Cai**[1], and **H Hong**[3]
[1]Institute of Engineering Thermophysics, Chinese Academy of Sciences, Beijing, People's Republic of China
[2]Graduate School, Chinese Academy of Sciences, Beijing, People's Republic of China
[3]Mechanical School, University of Science and Technology Beijing, Beijing, People's Republic of China

The manuscript was received on 20 July 2005 and was accepted after revision for publication on 9 January 2006.

DOI: 10.1243/09576509JPE215

Abstract: In this article, an innovative oxy-fuel power cycle is proposed as a promising CO_2 emission mitigation solution. It includes two cases with different characteristics in the cycle configuration. Case 1 basically consists of a water steam Rankine cycle and a steam-CO_2 recuperative-reheat cycle. Case 2 integrates some characteristics of Case 1 and a top Brayton cycle. The thermodynamic performances for the design conditions of these two cases were analysed using the advanced process simulator Aspen Plus and the results are given in detail. The corresponding exergy loss analyses were carried out to gain an understanding of the loss distribution. The MATIANT cycle, the CES cycle, and the GRAZ cycle were also evaluated as references. The results demonstrate that the proposed cycle has notable advantages in thermal efficiency, specific work, and technical feasibility compared with the reference cycles. For example, the thermal efficiency of Case 2 is 6.58 percentage points higher than that of the MATIANT cycle.

Keywords: oxy-fuel cycle, zero emission, CO_2 capture

1 INTRODUCTION

Worldwide efforts devoted to the research of zero-emission power plants have promoted the rapid development of related concepts, theories, and technologies [**1**, **2**]. Among these concepts, oxy-fuel combustion (internal combustion of fossil fuel with pure oxygen) is a characteristic and promising one. It has inspired some new thermodynamic cycles that are quite different from the current power systems. The most representative cycles of the oxy-fuel concept are the CES cycle [**3**–**6**], which is named the 'Water cycle' in references [**1**] and [**2**], the MATIANT cycle [**7**–**11**], and the GRAZ cycle [**12**–**14**]. The CES series includes the baseline cycle, the optimized baseline cycle, the cycle with double reheat and nitrogen integration, etc. [**5**]. The GRAZ series includes the GRAZ cycle and the S-GRAZ cycle. The CES series and the GRAZ series use the method of expanding to negative pressures to acquire high expansion ratios of turbines. However, the MATIANT series (MATIANT, E-MATIANT, CC-MATIANT) uses multistage compression (three to four stages) with intercooling to achieve the same effects. Apparently, the former offer better technical feasibility. The CES series utilizes the acquired high expansion ratios by reheating. But the outlet temperatures of the first combustor and the second combustor are different. The GRAZ series utilizes the acquired high expansion ratios by intermediate recuperation, which means putting the recuperator or the heat recovery steam generator (HRSG) between an intermediate pressure turbine (IPT) and a low-pressure turbine (LPT). According to references [**1**, **2**], these three types of cycles seem to have rather similar thermodynamic performances, and they are comparable to the currently available CO_2 capture technology (exhaust gas scrubbing by amine absorption in combined cycle power plants). They have much lower thermal efficiencies than do the 'emerging technology concepts' in reference [**1**] such as the SOFC + GT and the MSR-H2. Therefore, although the oxy-fuel concept provides an opportunity to develop zero-emission cycles with high efficiency, these three existing cycles do not fully exhibit its potential.

Corresponding author: Graduate School, Chinese Academy of Sciences, PO Box 2706, Beijing 100080, People's Republic of China. email: gch6969@yahoo.com.cn

On the basis of the above-mentioned background, this article proposes an innovative oxy-fuel cycle, which includes two cases. The proposed cycle is compared with other existing oxy-fuel cycles in the aspect of thermodynamic performances. The comparison with the CES cycle and the MATIANT cycle is grounded on simulations performed with similar computational assumptions. The evaluation of the GRAZ cycle is based on literature statements only. The results demonstrate that the proposed cycle has notable advantages in thermal efficiency, specific work, and technical feasibility relative to the reference cycles.

2 BASIC COMPUTATIONAL ASSUMPTIONS

Thermodynamic simulations were carried out with the assumptions listed in Table 1. In addition, the PENG-ROB equation was applied for the property of working fluid. Heat loss, including blade-cooling loss caused a total cycle efficiency penalty of 2 per cent. The produced CO_2 was compressed to 300 bar for further use or storage. The simulations were carried out using the commercial Aspen Plus code. The minimum heat exchange temperature difference $\Delta T_{\min}$ for gas/liquid was quite large in this study (30 °C). This was because the pressures of the exhaust gases were relatively low (0.105 bar) in the CES cycle and the proposed cycle. In reference [**1**], the $\Delta T_{\min}$ of gas/liquid heat exchange was 20 °C, where the corresponding pressure was 0.045 bar.

Table 1 Computational assumptions

Isentropic efficiency of compressors C1 and C2	0.87
Isentropic efficiency of compressors C3 and C4	0.85
Isentropic efficiency of the CH_4 and O_2 compressors	0.75
Isentropic efficiency of pumps	0.75
Isentropic efficiency of the HPT in the CES cycle	0.87
Isentropic efficiency of the HPT in the MATIANT cycle and the proposed cycle	0.85
Isentropic efficiency of IPT and LPT	0.90
Mechanical efficiency	0.99
Atmosphere temperature (ISO standard condition)	15 °C
Compression intercooler and condenser temperature	27 °C
CH_4 delivery temperature	15 °C
CH_4 delivery pressure	3 bar
LHV of CH_4	50.175 MJ/kg (802.802 kJ/mol)
O_2 delivery temperature	15 °C
O_2 delivery pressure	5 bar
Specific work for air separation	900 kJ/kgO_2 (0.25 kWh/kg)
Combustor pressure drop	3%
Heat exchanger pressure drop	5%
Heat exchanger $\Delta T_{\min}$ for gas/gas	30 °C
Heat exchanger $\Delta T_{\min}$ for gas/liquid	30 °C

3 PROPOSED CYCLE

3.1 Case 1

A flowsheet diagram of Case 1 is shown in Fig. 1. Figure 2 is the corresponding T–s diagram. Liquid water (1) is pumped to 44 bar (2). Then it is split into two branches. The flow (3), 38.27 per cent by mass of the flow (2), is injected into the first combustor directly. The flow (4) is further pumped to 189.47 bar. Then it (5) enters the HRSG to be vaporized and superheated. The steam (6), after driving the high-pressure turbine (HPT), enters the first combustor, which is operated at 40 bar. CH_4 (10), 63.45 per cent by mass of total fuel, together with the stoichiometric mass flow of O_2 (8) is also fed into the first combustor after being compressed. The high-temperature fluid (12) exiting the combustor at a mean temperature of 1300 °C is expanded in the IPT. After that, the flow (13) is reheated by firing with additional CH_4 and O_2 in the second combustor. The reheat pressure was set to 2.0 bar. The reheat temperature was 1300 °C. The stream (16) is then expanded to 0.11 bar in the LPT. The fluid (17) enters the HRSG to exchange heat with the stream (5) and is cooled down (18). Next, it flows into the condenser to be separated. The gas fluid (19) from the condenser contains 85.5 per cent CO_2 by mass, which is equal to the produced CO_2. It is then compressed to 1.05 bar (20). After cooling and water extraction, the CO_2 fluid (22) is further compressed with intercooling to a pressure of 300 bar (28). One part of the liquid water from the condenser is extracted out of the system as combustion product (30). The other part (1) is reconducted into the cycle. It was assumed that the pressure ratios of C2 and C3 were equal (8.88) to simplify the analyses.

The thermal parameters of Case 1 are listed in Table 2. This article presents the flowsheet diagram in detail, and lists the temperatures, pressures,

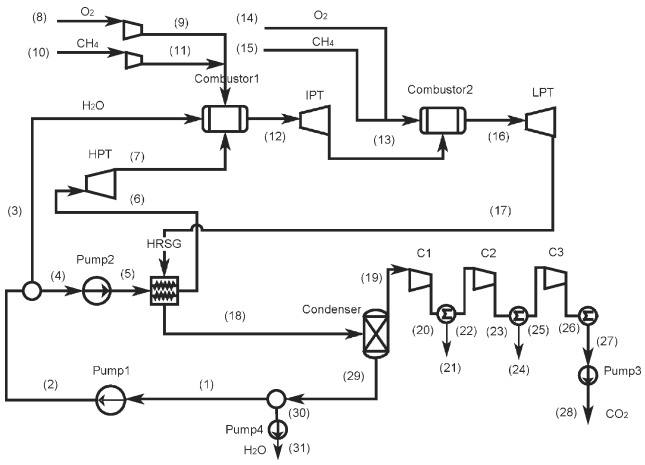

Fig. 1 Flowsheet diagram of Case 1

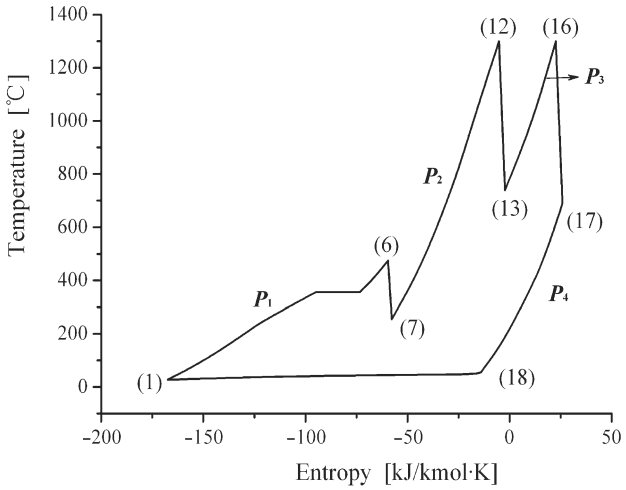

Fig. 2 *T*–*s* diagram of Case 1

vapour fractions, and CO_2 mole fractions of all points in this table. The information will help the reader to better evaluate the results.

The reheat pressure P_3 (Fig. 2) is optimized for maximum cycle net efficiency. The net efficiency is defined as

$$\eta = \frac{W_{\text{net}}}{\dot{m}_{\text{fuel}} \cdot \text{LHV}}$$

Table 2 Thermal parameters of Case 1

Points	Temperature (°C)	Pressure (bar)	Vapour fraction	Mole fraction of CO_2
(1)	27	0.1	0	0
(2)	27.4	44	0	0
(3)	27.4	44	0	0
(4)	27.4	44	0	0
(5)	28.7	189.47	0	0
(6)	542.2	180	1	0
(7)	313.9	40	1	0
(8)	15	5	1	0
(9)	311.2	40	1	0
(10)	15	3	1	0
(11)	281.5	40	1	0
(12)	1300	38.8	1	0.075
(13)	703.3	2	1	0.075
(14)	15	5	1	0
(15)	15	3	1	0
(16)	1300	1.94	1	0.104
(17)	724.7	0.11	1	0.104
(18)	59.2	0.105	1	0.104
(19)	27	0.1	1	0.707
(20)	249.4	1.05	1	0.707
(21)	27	1	0	0
(22)	27	1	1	0.97
(23)	221.8	8.88	1	0.97
(24)	27	8.436	0	0
(25)	27	8.436	1	0.996
(26)	233.6	75	1	0.996
(27)	27	71.25	0	0.996
(28)	72.6	300	1	0.996
(29)	27	0.1	0	0
(30)	27	0.1	0	0
(31)	27	1	0	0

where W_{net} is the cycle net power and $\dot{m}_{\text{fuel}}$ the mass flowrate of CH_4. The constraints for the optimization computation are as follows.

$P_1 = 189.47$ bar; $P_2 = 40$ bar; $P_4 = 0.11$ bar; the turbine inlet temperature (TIT) of the IPT and the LPT = 1300 °C.

The results, illustrated in Fig. 3, show that the net efficiency is at its maximum of 47.12 per cent when P_3 is equal to 2.0 bar. The choice of the values of the constraints for the optimization is based not only on thermal efficiency but also on technical feasibility. For example, P_4 was set to 0.11 bar to avoid the system operating at too high of a vacuum level, although the thermal efficiency would further increase if P_4 was lower. P_1 was set to 189.47 bar to limit the inlet pressure of the HPT to 180 bar.

3.2 Case 2

A flowsheet diagram of Case 2 is shown in Fig. 4. Figure 5 is the corresponding *T*–*s* diagram. Liquid water (1) is first pumped to 189.47 bar. Then it (2) enters the HRSG to be vapourized and superheated. The steam (3), after driving the HPT, enters the first combustor, which is operated at 40 bar as in Case 1. CH_4 (7), 38.73 per cent by mass of total fuel, together with the stoichiometric mass flow of O_2 (5) is also fed into the first combustor after being compressed. The high temperature fluid (9) exiting the combustor at a mean temperature of 1300 °C is expanded in the IPT. After that, the flow (10) is reheated by firing with additional CH_4 and O_2 in the second combustor. The reheat pressure was set to 2.0 bar. The reheat temperature was 1300 °C. The stream (13) is then expanded to 0.11 bar in the LPT. The fluid (14) enters the HRSG to exchange heat with the stream (2) and is cooled down. Next, it

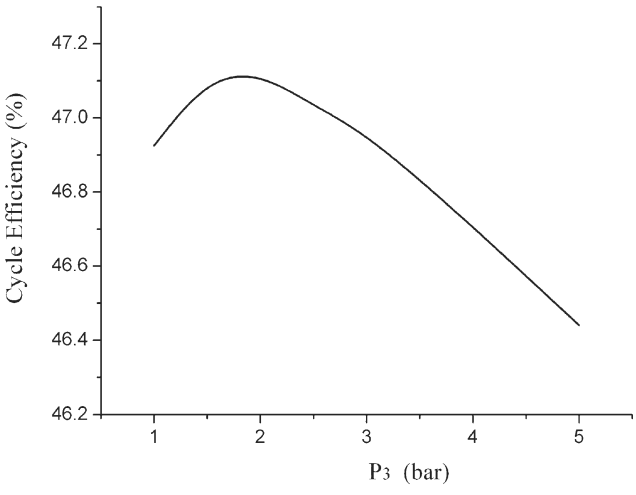

Fig. 3 Net efficiency of Case 1

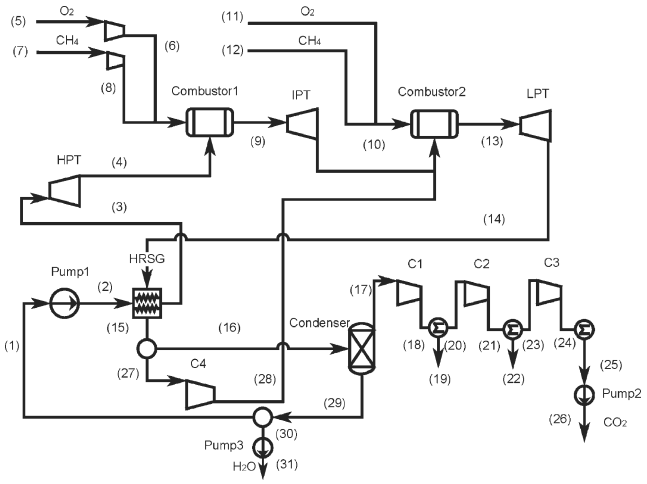

Fig. 4 Flowsheet diagram of Case 2

(15) is split into two branches. The flow (27), 36.13 per cent by mass of the flow (15), is delivered to C4. The exiting flow (28), which is at 437.0 °C and 2.0 bar, is sent back into the second combustor. The stream (16) enters the condenser to be separated. The gas fluid (17) from the condenser contains 85.5 per cent CO_2 by mass, which is equal to the produced CO_2. It is then compressed to 1.05 bar (18). After cooling and water extraction, the CO_2 fluid (20) is further compressed with intercooling to a pressure of 300 bar (26). One part of the liquid water from the condenser (30) is extracted out of the system as combustion product. The other part (1) is reconducted into the cycle. It was assumed that the pressure ratios of C2 and C3 were equal (8.88), as in Case 1.

The thermal parameters of Case 2 are listed in Table 3. Figure 6 shows the variation of the net efficiency with the reheat pressure P_3. The constraints for the optimization computation are as follows.

Table 3 Thermal parameters of Case 2

Points	Temperature (°C)	Pressure (bar)	Vapour fraction	Mole fraction of CO_2
(1)	27	0.1	0	0
(2)	28.7	189.47	0	0
(3)	544.4	180	1	0
(4)	315.9	40	1	0
(5)	15	5	1	0
(6)	311.2	40	1	0
(7)	15	3	1	0
(8)	281.5	40	1	0
(9)	1300	38.8	1	0.054
(10)	701	2	1	0.054
(11)	15	5	1	0
(12)	15	3	1	0
(13)	1300	1.94	1	0.111
(14)	725.3	0.11	1	0.111
(15)	59.1	0.105	1	0.111
(16)	59.1	0.105	1	0.111
(17)	27	0.1	1	0.707
(18)	249.4	1.05	1	0.707
(19)	27	1	0	0
(20)	27	1	1	0.97
(21)	221.8	8.88	1	0.97
(22)	27	8.436	0	0
(23)	27	8.436	1	0.996
(24)	233.6	75	1	0.996
(25)	27	71.25	0	0.996
(26)	72.6	300	0	0.996
(27)	59.1	0.105	1	0.111
(28)	437	2	1	0.111
(29)	27	0.1	0	0
(30)	27	0.1	0	0
(31)	27	1	0	0

$P_1 = 189.47$ bar; $P_2 = 40$ bar; the TIT of the IPT and the LPT = 1300 °C; $P_4 = 0.11$ bar.

Figure 6 shows that the net efficiency is at its maximum of 50.64 per cent when P_3 is equal to 2.0 bar. The criteria for setting constraints are the same as in Case 1.

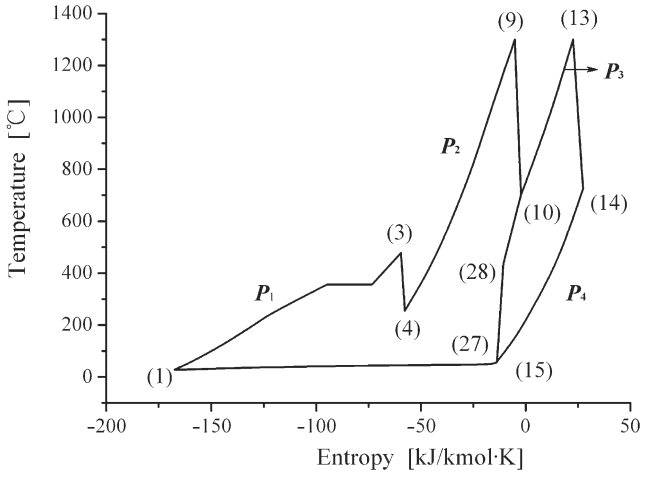

Fig. 5 *T*–*s* diagram of Case 2

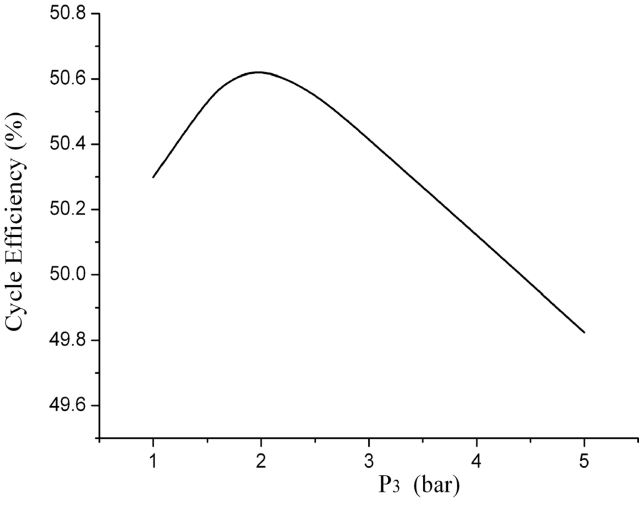

Fig. 6 Net efficiency of Case 2

4 MATIANT CYCLE

A flowsheet diagram of the MATIANT cycle [**8**] is shown in Fig. 7. Figure 8 is the corresponding T–s diagram. The working fluid (1), containing 98.75 per cent CO_2 and 1.25 per cent H_2O by mass, is compressed by C1–C3 with intercooling to 75 bar. Then it (8) enters the condenser to be liquefied. Next the liquid CO_2 (9) is pumped to 300 bar. The flow (10), after the combustion product is extracted, enters the recuperator to become superheated and supercritical CO_2 steam. The fluid (13) at 600 °C and 285 bar, after driving the HPT, is returned back into the recuperator. The flow (15) exiting the recuperator enters the first combustor, which is operated at 40 bar. CH_4 (18), 64.99 per cent by mass of total fuel, together with the stoichiometric mass flow of O_2 (16) is also fed into the first combustor after being compressed. The high-temperature fluid (20) exiting the combustor at a mean temperature of 1300 °C is expanded in the IPT. The flow (21), after that, is reheated by firing with additional CH_4 and O_2 in the second combustor. The reheat pressure was set to 9.03 bar. The reheat temperature was 1300 °C. The stream (26) is then expanded to 1.1 bar in the LPT. The fluid (27) enters the recuperator to exchange heat with streams (12) and (14). Next, it (28) flows into the condenser to be separated. The gas fluid (1) from the condenser is then recycled to the compressors. It was assumed that the pressure ratios of C1–C3 were equal (4.36) to simplify the analyses.

The thermal parameters of the MATIANT cycle are listed in Table 4. Figure 9 shows the variation of the net efficiency with the reheat pressure P_3. The constraints for the optimization computation are as follows.

$P_1 = 300$ bar; $P_2 = 40$ bar; the TIT of the IPT and the LPT = 1300 °C; $P_4 = 1.1$ bar; the temperature of point (13) = 600 °C; $\Delta T_{\min}$ in the recuperator = 30 °C.

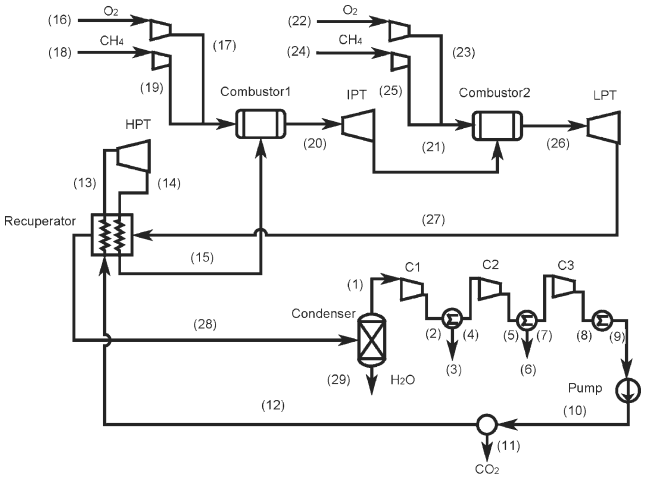

Fig. 7 Flowsheet diagram of the MATIANT cycle

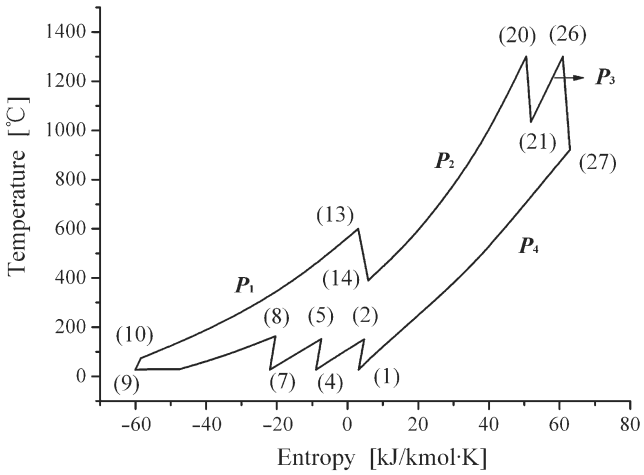

Fig. 8 T–s diagram of the MATIANT cycle

According to reference [**8**], the temperature of point (15) should be limited to 700 °C. Therefore, the net efficiency and the corresponding temperature of point (15) are denoted by dashed lines in Fig. 9 when the temperature is greater than 700 °C. The figure shows that the net efficiency is at its maximum of 44.06 per cent when P_3 is equal to 9.03 bar. The corresponding temperature of point (15) is 700 °C. The criteria for setting constraints are based on reference [**8**].

Table 4 Thermal parameters of the MATIANT cycle

Points	Temperature (°C)	Pressure (bar)	Vapour fraction	Mole fraction of CO_2
(1)	27	1	1	0.97
(2)	151.5	4.36	1	0.97
(3)	27	4.142	0	0
(4)	27	4.142	1	0.993
(5)	153.7	18.059	1	0.993
(6)	27	17.156	0	0
(7)	27	17.156	1	0.998
(8)	163.1	75	1	0.998
(9)	27	71.25	0	0.998
(10)	73.4	300	1	0.998
(11)	73.4	300	1	0.998
(12)	73.4	300	1	0.998
(13)	600	285	1	0.998
(14)	390.4	42.1	1	0.998
(15)	700	40	1	0.998
(16)	15	5	1	0
(17)	311.2	40	1	0
(18)	15	3	1	0
(19)	281.5	40	1	0
(20)	1300	38.8	1	0.908
(21)	1029.2	9.03	1	0.908
(22)	15	5	1	0
(23)	84.7	9.03	1	0
(24)	15	3	1	0
(25)	121.8	9.03	1	0
(26)	1300	8.76	1	0.87
(27)	925.8	1.1	1	0.87
(28)	103.4	1.05	1	0.87
(29)	27	1	0	0

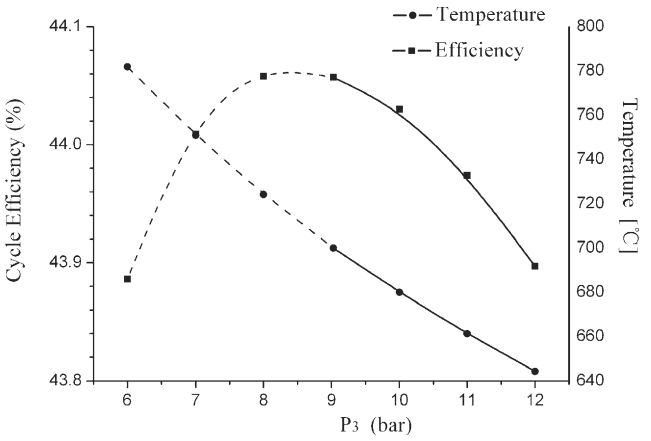

Fig. 9 Net efficiency and temperature of point (15) of the MATIANT cycle

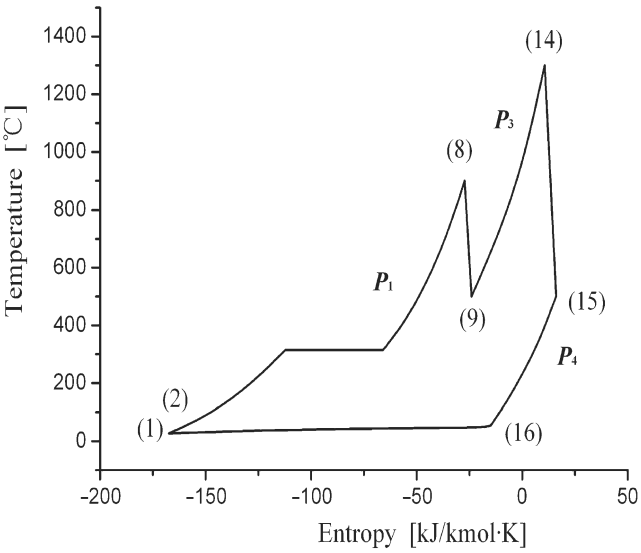

Fig. 11 T–*s* diagram of the CES cycle

5 CES CYCLE

A flowsheet diagram of the CES cycle (Case 2 in reference [**5**] – optimized baseline cycle) is shown in Fig. 10. Figure 11 is the corresponding *T*–*s* diagram. Liquid water (1) is pumped to 112.2 bar. Then it (2) enters the recuperator to be preheated. The fluid (3) flows into the first combustor (gas generator), which is operated at 106.6 bar. CH_4 (6), 52.63 per cent by mass of total fuel, together with the stoichiometric mass flow of O_2 (4) is also fed into the first combustor after being compressed. The intermediate temperature fluid (8) exiting the combustor at a mean temperature of 900 °C is expanded in the HPT. After that, the flow (9) is reheated by firing with additional CH_4 and O_2 in the second combustor. The reheat pressure was set to 9.9 bar. The reheat temperature was 1300 °C. The stream (14) then is expanded to 0.11 bar in the LPT. The fluid (15) enters the recuperator to exchange heat with the stream (2) and is cooled down (16). Next, it enters the condenser to be separated. The gas fluid (17) from the condenser contains 85.5 per cent CO_2 by mass, which is equal to the produced CO_2. It is then compressed to 1.05 bar (18). After cooling and water extraction, the CO_2 fluid (20) is further compressed with intercooling to a pressure of 300 bar (26). One part of the liquid water from the condenser is extracted out of the system as combustion product

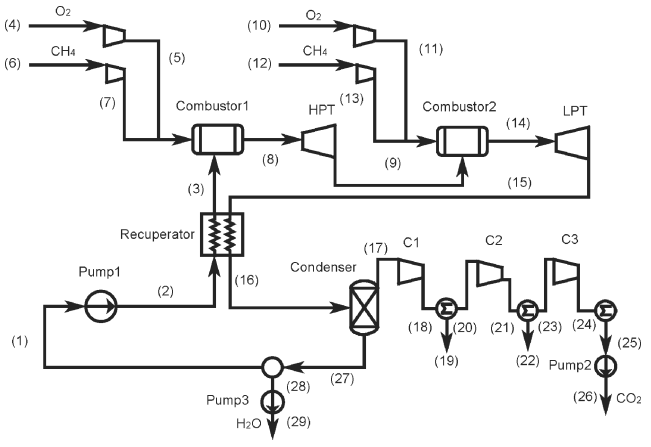

Fig. 10 Flowsheet diagram of the CES cycle

Table 5 Thermal parameters of the CES cycle

Points	Temperature (°C)	Pressure (bar)	Vapour fraction	Mole fraction of CO_2
(1)	27	0.1	0	0
(2)	28	112.2	0	0
(3)	283.3	106.6	0	0
(4)	15	5	1	0
(5)	506.2	106.6	1	0
(6)	15	3	1	0
(7)	394.7	106.6	1	0
(8)	900	103.4	1	0.061
(9)	509	9.9	1	0.061
(10)	15	5	1	0
(11)	96.6	9.9	1	0
(12)	15	3	1	0
(13)	131.2	9.9	1	0
(14)	1300	9.603	1	0.099
(15)	493.3	0.11	1	0.099
(16)	58	0.105	1	0.099
(17)	27	0.1	1	0.707
(18)	249.4	1.05	1	0.707
(19)	27	1	0	0
(20)	27	1	1	0.97
(21)	221.8	8.88	1	0.97
(22)	27	8.436	0	0
(23)	27	8.436	1	0.996
(24)	233.6	75	1	0.996
(25)	27	71.25	0	0.996
(26)	72.6	300	1	0.996
(27)	27	0.1	0	0
(28)	27	0.1	0	0
(29)	27	1	0	0

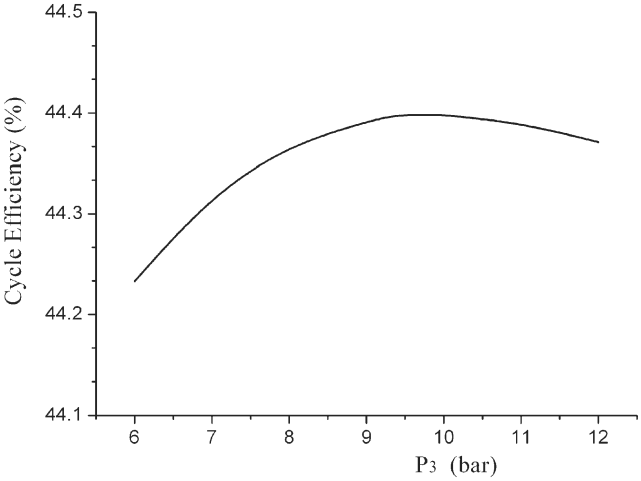

Fig. 12 Net efficiency of the CES cycle

(28). The other part (1) is reconducted into the cycle. It was assumed that the pressure ratios of C2 and C3 were equal (8.88) to simplify the analyses.

The thermal parameters of the CES cycle are listed in Table 5. Figure 12 shows the variation of the net efficiency with the reheat pressure P_3. The constraints for the optimization computation are as follows.

$P_1 = 106.6$ bar; $P_4 = 0.11$ bar; the TIT of the HPT = 900 °C; the TIT of the LPT = 1300 °C.

The figure shows that the net efficiency is at its maximum of 44.40 per cent when P_3 is equal to 9.9 bar. The criteria for setting constraints are mainly based on reference [**5**]. The TIT of the HPT was set to 900 °C [**1**], which is a little higher than 816 °C in reference [**5**]. P_4 was set to 0.11 bar for comparison with Case 1 and Case 2 of the proposed cycle.

6 COMPARISON

The exergy loss was analysed to gain an understanding of the loss distribution. The results, based on per mole of CH_4 consumed, are listed in Table 6. The net input exergy in this table is defined as

$$\text{Net input exergy} = \text{Exergy } (CH_4) + \text{Exergy } (O_2) - \text{Exergy } (CO_2) - \text{Exergy } (H_2O)$$

in which Exergy (CH_4) is the total input exergy of CH_4; Exergy (O_2) is the total input exergy of O_2; Exergy (CO_2) and Exergy (H_2O) are the total exergy of combustion-produced CO_2 and H_2O exiting the systems, respectively. CFO denotes the processes of CH_4 and O_2 compression. ASUHL denotes the air separation process and heat loss. HEX denotes all heat exchange, intercooling, and condensation processes. The net output work is the net work of the whole power cycle, including the air separation unit.

The results show that the exergy losses were mainly distributed in the combustion, HEX, and ASUHL processes. The ranking of the combustion exergy losses were: (a) CES (35.8 per cent); (b) Case 1 (34.66 per cent); (c) Case 2 (29.32 per cent); (d) MATIANT (25.94 per cent). The ranking of the HEX exergy losses were: (a) MATIANT (14.28 per cent); (b) Case 2 (7.21 per cent); (c) CES (7.13 per cent); (d) Case 1 (6.40 per cent). The exergy losses of ASUHL were almost the same in different systems. In addition, the exergy losses of the compression processes of the MATIANT cycle were also significant. This is because of the relatively high mass flowrate passing through the compressors. The advantage of Case 2 compared with Case 1 comes mainly from the combustion processes. The

Table 6 Exergy analyses of various cycles

Cycle name		Case 1		Case 2		MATIANT		CES	
Item		Exergy (kJ/mol-CH_4)	Per cent	Exergy (kJ/mol-CH_4)	Per cent	Exergy (kJ/mol-CH_4)	Per cent	Exergy (kJ/mol-CH_4)	Per cent
LHV of CH_4		802.80		802.80		802.80		802.80	
Net input exergy		819.04	100	819.21	100	819.07	100	819.04	100
Exergy losses	C1–C4	2.59	0.32	7.88	0.96	20.96	2.56	2.59	0.32
	CFO	2.73	0.33	1.67	0.20	3.40	0.42	3.90	0.48
	Pump	0.85	0.10	0.81	0.10	6.40	0.78	0.71	0.08
	Combustor 1	201.47	24.59	95.30	11.63	140.59	17.29	184.78	22.56
	Combustor 2	82.49	10.07	144.97	17.69	70.87	8.65	108.47	13.24
	HPT	2.61	0.32	3.83	0.47	11.79	1.44	9.40	1.15
	IPT	10.40	1.27	8.73	1.07	8.05	0.98		
	LPT	11.28	1.38	16.53	2.02	12.49	1.52	20.40	2.49
	HEX	52.44	6.40	59.11	7.21	116.96	14.28	58.49	7.13
	ASUHL	73.86	9.02	73.86	9.02	73.86	9.02	73.86	9.02
Net output work		378.31	46.19	406.52	49.62	353.69	43.18	356.43	43.52
Output exergy		819.03	99.99	819.21	99.99	819.06	99.99	819.04	99.99

Table 7 Net efficiency and specific work

Cycle name	Net efficiency (%)	Specific work (kJ/kg)
Case 1	47.12	1900.43
Case 2	50.64	1383.62
MATIANT	44.06	560.05
CES	44.40	1716.65

corresponding exergy losses of the former were 5.34 percentage points less than that of the latter.

Table 7 shows the thermodynamic performances of these three cycles based on the computational results of the previous paragraphs. The specific work is defined as

$$\text{Specific work} = \frac{W_{\text{net}}}{\dot{m}_{\max}}$$

in which $\dot{m}_{\max}$ is the mass flowrate exiting the LPT.

The thermal efficiency is a crucial aspect when evaluating and comparing different thermodynamic cycles. However, the technical feasibility and the specific work are also very important. This is because they can, just as the thermal efficiency, directly affect the economics.

The MATIANT cycle has the lowest thermal efficiency and the lowest specific work among all these three cycles. But some thermal parameters of this cycle are more notable. For example, the working fluid (12) in Fig. 7 at a pressure of 300 bar is heated to 600 °C in the recuperator. The stream (14) is heated to 700 °C at 40 bar in the recuperator. The exhaust gas side inlet temperature of the recuperator is as high as 925.8 °C. The pressure of the working fluid (8) is as high as 75 bar at the outlet of the C3 compressor. Therefore, the working conditions of the recuperator and the compressors are also the worst among these three cycles.

Accordingly, the advantages of the proposed cycle compared with the MATIANT cycle are as follows.

1. The proposed cases have higher efficiencies. The thermal efficiency of Case 1 is 3.06 percentage points higher than that of the MATIANT cycle. The thermal efficiency of Case 2 is 6.58 percentage points higher than that of the MATIANT cycle.
2. The proposed cases have higher specific works. The specific work of Case 1 is 3.39 times of that of the MATIANT cycle. The specific work of Case 2 is 2.47 times of that of the MATIANT cycle.
3. The working conditions of heat exchangers in the proposed cases are better and the request for expensive high temperature material is lower.
4. The working conditions of compressors in the proposed cases are better. In Case 1, the working fluid is compressed by a pump. Therefore, the part-load characteristics should be excellent. In Case 2, the working fluid compressor (C4) has a lower pressure ratio when compared with C1–C3 in the MATIANT cycle. The mass flowrate passing through C4 is also lower. If C4 in Case 2 was driven by a motor as C1–C3 in the MATIANT cycle [**8**], the required motor would also be cheaper.
5. The proposed cases are closer to the concept of zero-emission than the MATIANT cycle. Leaking of working fluid in semiclosed thermodynamic cycles is inevitable. The highest pressure of the MATIANT cycle is as high as 300 bar, which is higher than that (180 bar) of the proposed cases. The specific work is lower, which means the working fluid mass flowrate is higher. The mass flowrate exiting the LPT is 14.34 times of the combustion-produced CO_2. However, the corresponding mass flowrates of Case 1 and Case 2 are 4.52 and 6.67 times of the combustion-produced CO_2, respectively. The concentration of CO_2 in the working fluid of the MATIANT cycle is also higher than that of the proposed cases. The MATIANT cycle is more complicated in configuration and involves many internal heat exchange processes. Consequently, leaking of CO_2 in the MATIANT cycle could be more serious than that in the proposed cycle and the CES cycle. If the leakage of working fluid accounted for 1 per cent of the mass flowrate exiting the LPT, 13.51 per cent by mass of combustion-produced CO_2 would be discharged into the environment. Therefore, the MATIANT cycle can only be called a near-zero emission cycle. In contrast, the highest pressures of the proposed cycle and the CES cycle are lower. The working fluid in the high pressure section is pure water/steam. There are fewer heat exchange processes. The concentration of CO_2 in the working fluid is also lower. Therefore, leaking has little effect on the recovery of CO_2.

Two cycles, namely the E-MATIANT and the CC-MATIANT [**11**] have been developed based on the MATIANT cycle. The E-MATIANT cycle is in essence an intercooled recuperative gas turbine cycle. The most noteworthy parameters of this cycle are as follows. The combustor is operated at 60 bar and 1300 °C; the working fluid is compressed in a four-staged compressor with intercoolers. The CC-MATIANT cycle is very close to an oxy-fuel combined cycle. The most notable parameters of the CC-MATIANT cycle are as follows. The outlet temperature of the compressor is above 500 °C; the exhaust gas side inlet temperature of the recuperator is as high as 900–1000 °C. The thermal efficiencies of the E-MATIANT and the CC-MATIANT cycle are 47 and 49 per cent, respectively. Obviously, the working conditions of these cycles are not favourable.

The CES cycle has a rather uncomplicated cycle configuration, especially when compared with the MATIANT cycle. The working fluid is compressed by a pump. Therefore, the part-load characteristics should be excellent. However, the CES series always adopts the manner of reheating with different outlet temperature of combustors. This manner, on the one hand, increases the combustion exergy losses and on the other hand increases the compression work of CH_4 and O_2. Therefore it is not beneficial. The thermal efficiency of Case 1 is 2.72 percentage points higher when compared with the CES cycle. The specific work is also slightly higher. The thermal efficiency of Case 2 is 6.24 percentage points higher than that of the CES cycle but the specific work is relatively lower.

The advantages of Case 1 when compared with the CES cycle mainly comes from the following features.

1. The manner of reheating with the same outlet temperatures of the two combustors is adopted in Case 1. Accordingly, the combustion exergy losses and the work of CH_4 and O_2 compression are less.
2. Only a part of the recycled liquid water (flow (5) in Fig. 1) enters the HRSG. Therefore, this flow can be vapourized and superheated by the exhaust gas, which makes it possible to arrange a Rankine cycle (flow (5) to (7) in Fig. 1) in front of the first combustor. But in the CES cycle, the recycled working fluid (flow (3) in Fig. 7) is still in liquid phase after exchanging heat with the exhaust gas, and therefore it is not able to do work by direct expansion.

The thermal efficiency of the GRAZ cycle is 1.4 percentage points lower than that of the CES cycle according to the computational assumptions and results in reference [**1**]. It is also the lowest among the nine concepts for natural gas-fired power plants with CO_2 capture. This is partly because of the adoption of intermediate recuperation in the GRAZ cycle. After the recuperation, the capacity of the working fluid for work is rather low, and thus the corresponding expansion ratios are not utilized efficiently [**15**]. The computational assumptions and results in reference [**14**] indicate that the thermal efficiency of the S-GRAZ cycle is 2.8 percentage points higher than that of the GRAZ cycle (when firing with CH_4). The S-GRAZ cycle retains the feature of intermediate recuperation and the increase of thermal efficiency is not remarkable. The most notable parameters of the S-GRAZ cycle are as follows. The compression ratio is as high as 40. The outlet temperature of the C2 compressor (see Fig. 2 in reference [**14**]) is 600 °C when the isentropic efficiency is 0.88. Therefore, the working conditions of the compressors are also not good.

Although the MATIANT cycle has the worst technical feasibility of the above-mentioned oxy-fuel cycles, it has to be pointed out that compared with 'emerging technology concepts' in reference [**1**] such as the SOFC + GT and the MSR-H2, the MATIANT cycle is indeed quite realistic. That is because oxy-fuel cycles in nature are very close to current mature gas turbine power systems. And they are commonly more suitable for large-scale applications. Taking the CES cycle as an example, the core component of the CES cycle, namely the gas generator, was tested on the laboratory scale in early 2001 [**16**], and on 20 MW scale in 2002–2003 [**17**]. The results demonstrated good reliability and stability. Furthermore, the CES cycle has been functioning in a demonstration power plant and exporting power to the electrical grid since late 2004. In addition, the design of a prototype plant of the GRAZ cycle was reported in reference [**13**]. Oxy-fuel cycles can also completely eliminate other atmospheric emissions such as NO_x.

The energy required for oxygen production is an important factor that influences the thermal efficiency of oxy-fuel cycles. It leads to an efficiency penalty of 7.2 percentage points with the computational assumptions of this study. However, it is possible to integrate the air separation unit with the power unit to improve the overall performances (see Case 3 in reference [**5**] – cycle with double reheat and nitrogen integration). At the same time the progress of novel technologies for air separation is very promising. For example, different consortia are developing ionic transport membrane technology with DOE and EU funding for commercialization by 2008–2009 [**18**]. In addition, some oxy-fuel cycles integrating liquefied natural gas (LNG) evaporation processes with air separation or CO_2 liquefaction processes were proposed recently [**19–21**]. The energy required for oxygen production or CO_2 compression is decreased notably in these systems by utilizing LNG cryogenic exergy efficiently.

Compared with other concepts of zero emission, the oxy-fuel concept not only has the advantage of technical feasibility, but also the potential for improving thermodynamic performances. Therefore, it is a promising and competitive solution for CO_2 emission mitigation.

7 CONCLUSIONS

This article presents a novel oxy-fuel gas turbine cycle that includes two cases with different characteristics in cycle configuration. The thermal efficiency and the specific work of Case 1 at the design conditions are 47.12 per cent and 1900.43 kJ/kg, respectively. The thermal efficiency and the specific

work of Case 2 at the design conditions are 50.64 per cent and 1383.62 kJ/kg, respectively. Compared with the reference cycles, namely the MATIANT cycle, the CES cycle, and the GRAZ cycle, the advantages of these two cases in thermodynamic performances and technical feasibility are remarkable. There are several ways to further improve the performances of the proposed cycle. For example, the thermal efficiency and the specific work would be higher if double reheat was applied. However, the cycle configuration would be more complicated. The economics might not be good. Therefore, these cases are not simulated in this study. The economic analyses, part-load characteristic investigation, and prototype plant design will be carried out in the near future.

ACKNOWLEDGEMENT

This work was supported by the Natural Science Foundation of China (grant no. 50520140517).

REFERENCES

1 **Kvamsdal, H., Maurstad, O., Jordal, K.,** and **Bolland, O.** Benchmarking of gas-turbine cycles with CO_2 capture. Presented as a Peer-reviewed Paper at the 7th International Conference on *Greenhouse gas control technologies*, Vancouver, Canada, September 2004.

2 **Bolland, O., Kvamsdal, H.,** and **Boden, J.** A thermodynamic comparison of the oxy-fuel power cycles Watercycle, Graz-cycle and MATIANT-cycle. Proceedings of the International Conference on *Power generation and sustainable development*, Liège, Belgium, October 2001.

3 **Anderson, R., Brandt, H., Mueggenburg, H., Taylor, J.,** and **Viteri, F.** A power plant concept which minimizes the cost of carbon dioxide sequestration and eliminates the emission of atmospheric pollutants. Proceedings of the 4th International Conference on *Greenhouse gas control technologies*, Interlaken, Switzerland, Pergamon, 1998, pp. 59–62.

4 **Anderson, R., Brandt, H., Doyle, S., Mueggenburg, H., Taylor, J.,** and **Viteri, F.** A unique process for production of environmentally clean electric power using fossil fuels. Proceedings of the 8th International Symposium on *Transport phenomena and dynamics of rotating machinery*, Honolulu, Hawaii, March 2000.

5 **Marin, O., Bourhis, Y., Perrin, N., Zanno, P., Viteri, F.,** and **Anderson, R.** High efficiency, zero emission power generation based on a high-temperature steam cycle. Proceedings of the 28th International Technical Conference on *Coal utilization and fuel systems*, Clearwater, Florida, US, March 2003.

6 **Smith, J. R., Surles, T., Marais, B., Brandt, H.,** and **Viteri, F.** Power production with zero atmospheric emissions for the 21st century. Proceedings of the 5th International Conference on *Greenhouse gas control technologies*, Cairns, Australia, August 2000.

7 **Iantovski, E.** and **Mathieu, Ph.** Highly efficient zero emission CO_2-based power plant. *Energ. Convers. Manage.*, 1997, **38**(9999), s141–s146.

8 **Mathieu, Ph.** and **Nihart, R.** Zero-emission MATIANT cycle. *Trans. ASME, J. Eng. Gas Turb. Power*, 1999, **21**(1), 116–120.

9 **Mathieu, Ph.** and **Nihart, R.** Sensitivity analysis of the MATIANT cycle. *Energ. Convers. Manage.*, 1999, **40**(15), 1687–1700.

10 **Mathieu, Ph., Dubuisson, R., Houyou, S.,** and **Nihart, R.** New concept of CO_2 removal technologies in power generation, combined with fossil fuel recovery and long term CO_2 sequestration. ASME Turbo Expo Conference, 2000-GT-0161, 2000.

11 **Houyou, S., Mathieu, Ph.,** and **Nihart, R.** Techno-economic comparison of different options of very low CO_2 emission technologies. Proceedings of the 5th International Conference on *Greenhouse gas control technologies*, Cairns, Australia, August 2000.

12 **Jericha, H.** and **Fesharaki, M.** The Graz cycle-1500 °C max temperature potential H_2-O_2 fired CO_2 capture with CH_4-O_2 firing. ASME paper 95-CTP-79. In ASME Cogen-Turbo Power Conference, Vienna, 1995.

13 **Jericha, H., Gottlich, E., Sanz, W.,** and **Heitmeir, F.** Design optimization of the Graz prototype plant. *Trans. ASME, J. Eng. Gas Turb. Power*, 2004, **126**(4), 733–740.

14 **Sanz, W., Jericha, H., Moser, M.,** and **Heitmeir, F.** Thermodynamic and economic investigation of an improved Graz cycle power plant for CO_2 capture. Proceedings of the *ASME Turbo Expo Conference*, 2004, Vol. 7, Paper No. GT-2004-53722.

15 **Cai, R.** and **Jiang, L.** Analysis of the recuperative gas turbine cycle with a recuperator located between turbines. *Appl. Thermal Eng.*, 2006, **26**, 89–96.

16 **Anderson, R.** *Development of a unique gas generator for a non-polluting power plant*. EISG Report on Project EISG 99-20, California Energy Commission Grant # 99-20, May 2001.

17 **Anderson, R., Baxter, E.,** and **Doyle, S.** *Fabricate and test an advanced non-polluting turbine drive gas generator*. Final Report, under DE Cooperative Agreement No. DE-FC26-00NT 40804, 1 September 2000 to 1 June 2003.

18 **Simmonds, M., Miracca, I.,** and **Gerdes, K.** Oxyfuel technologies for CO_2 capture: a techno-economic overview. Proceedings of the 7th International Conference on *Greenhouse gas control technologies*, Vancouver, Canada, September 2004.

19 **Velautham, S., Ito, T.,** and **Takata, Y.** Zero-emission combined power cycle using LNG cold. *JSME Int. J. Ser. B; Fluids Thermal Eng.*, 2001, **44**(4), 668–674.

20 **Zhang, N., Cai, R.,** and **Wang, W.** Study on near-zero CO_2 emission thermal cycles with LNG cryogenic exergy utilization. *ASME Int. Gas Turbine Inst. Publ. IGTI*, 2003, **3**, 329–337.

21 **Zhang, N.** and **Lior, N.** Configuration analysis of a novel zero CO_2 emission cycle with LNG cryogenic exergy utilization. *ASME Adv. Energy Syst. Div. Publ. AES*, 2003, **43**, 333–343.

APPENDIX

Notation

ASU	air separating unit
ASUHL	air separation process and heat loss
C1	compressor 1
C2	compressor 2
C3	compressor 3
C4	compressor 4
CFO	compression processes of CH_4 and O_2
HEX	all heat exchange, intercooling and condensation processes
HPT	high-pressure turbine
HRSG	heat recovery steam generator
IPT	intermediate pressure turbine
LHV	low heating value (MJ/kg)
LNG	liquefied natural gas
LPT	low-pressure turbine
$\dot{m}_{\text{fuel}}$	mass flowrate of CH_4 ($10^3 \times$ kg/s)
$\dot{m}_{\max}$	mass flowrate exiting the LPT (kg/s)
P_1	high pressure (bar)
P_2	upper intermediate pressure (bar)
P_3	lower intermediate pressure (bar)
P_4	low pressure (bar)
TIT	turbine inlet temperature (°C)
W_{net}	cycle net power (kW)
η	net thermal efficiency
$\Delta T_{\min}$	heat exchange minimum temperature difference (°C)